第34卷 第4期 焊 接 学 报 Vol. 34 No. 4
2013年4月 TRANSACTIONS OF THE CHINA WELDING INSTITUTION April 2013

基于超声信号和图像融合的焊缝缺陷识别

胡文刚， 刚 铁
(哈尔滨工业大学 先进焊接与连接国家重点实验室，哈尔滨 150001)

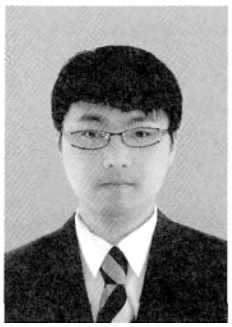

胡文刚

摘 要：超声无损检测已被广泛用来检测材料内部的缺陷，然而对缺陷性质的识别始终是检测的难点，为此研究了一种基于超声信号和图像融合的焊缝缺陷识别新方法. 该方法充分利用检测数据，通过对缺陷回波信号特征与缺陷形态特征的数据融合，实现了焊缝缺陷的有效识别. 利用自主研制的超声成像手动检测系统对含有气孔、夹渣、裂纹、未焊透和未熔合五类典型焊接缺陷的焊件进行了检测，分别提取缺陷的超声回波信号特征和缺陷图像的形态特征，构建神经网络实现超声信号和图像特征的数据融合. 结果表明，该方法实现了多类缺陷的识别，提高了缺陷识别率，有助于焊缝质量评定.

关键词：超声检测； 缺陷识别； 数据融合； 神经网络
中图分类号：TG115.28 **文献标识码**：A **文章编号**：0253－360X(2013)04－0053－04

0 序 言

在超声检测领域中，缺陷的定性识别是公认的难题之一，目前对缺陷的定性研究还没有获得满意的结果. 随着高科技的不断发展，各种超声检测技术应运而生，特别是超声成像技术的出现，它能够直观的反馈检测试件内部的缺陷分布图像，有效的提高无损检测的可靠性，在缺陷的定位和定量评定方面也取得了很大的进展，是定量无损检测的重要工具[1]. 但是在如何解释缺陷图像、提取和评价图像特征等方面目前还处于研究阶段，如何实现缺陷性质的智能识别仍然是超声检测研究领域中的难题之一[2]. 目前国内外对于大中型结构焊缝的现场在役检测及对缺陷性质的判断完全依靠检测人员的经验，带有很大的主观性，严重影响检测结果的可靠性，这给实际的检测带来诸多不便[3].

近年来，神经网络技术在数据融合领域得到了广泛的重视. 数据融合技术和神经网络技术都是对人脑综合处理复杂问题的一种模仿，从数据融合的角度来看，神经网络可以看作一个融合系统，利用神经元之间不同的连接方式可以构成不同的融合系统. 神经网络技术具有综合分析数据的能力，因而可以利用神经网络技术来实现数据融合. 文中选用BP神经网络作为融合分类器，对缺陷的超声信号特征与图像形态特征进行数据融合，实现多类缺陷的智能识别，有效的提高了缺陷的识别率.

收稿日期：2012－03－12
基金项目：国家自然基金资助项目(51175113，51105033)；国际合作资助项目(2007DFR70070)

1 试验方法

1.1 基于视频定位的检测系统

针对工业实际应用中存在的问题，以解决常规手动超声无损检测中缺陷无法直观显示和缺陷识别困难为首要目的，开发了一套基于USB摄像头视频定位的焊缝缺陷超声定位成像检测系统，图1是整个系统的硬件结构图.

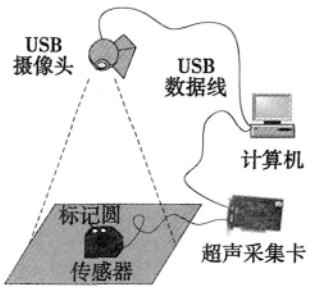

图1 基于视频定位的超声检测系统

Fig. 1 Ultrasonic testing system based on video positioning

系统选用了USB摄像头作为位置传感器，实时采集检测区域内的探头位置信息，进而实现了焊缝缺陷的连续扫查. 系统能够实时地记录探头的位置信号，以及实时存储探头扫查位置上的缺陷回波信

号. 通过 USB 接口进入计算机后被软件调用,实现对信号的处理,以获得缺陷的三维位置信息,以三视图的方式成像显示,直观的给出缺陷的位置、大小、分布和取向的形态特征,为后续缺陷的识别及焊缝质量的评估提供了可靠的数据[3].

1.2 试件制备与试验方法

为了检测实际的焊缝缺陷,首先制备了大量含有气孔、夹渣、裂纹、未焊透和未熔合 5 类典型焊接缺陷的对接焊缝试样. 焊接试件的材料选用低碳合金钢,钢板的厚度为 24 mm. 通过控制焊接工艺参数与焊接条件,采用焊条电弧焊与氩弧焊相结合的方法制备带自然缺陷的对接焊缝,焊后经 X 射线检测,符合试验要求. 试件的坡口形式为 X 形,尺寸示意图如图 2 所示.

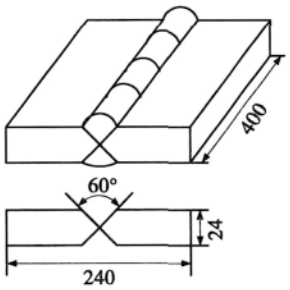

图 2 实际焊接试件尺寸及坡口形式示意图(mm)

Fig. 2 Schematic of dimension and root form of specimen

由于焊接余高的存在,对接焊缝一般不采用直探头进行手动检测,为此选用了斜探头对制备的对接焊缝试件进行检测. 为了确保检测结果的准确性,在检测前对超声波探头的相关参数进行了测量. 试验选用德国 KK 公司生产的 MBW70-4 斜探头,其参数如表 1 所示.

表 1 斜探头参数

Table 1 Parameter of angle beam probe

探头型号	晶片尺寸 a/mm	中心频率 f/MHz	探头延迟 t/μs	钢折射角 θ/(°)	前沿距离 c/mm
MBW70-4	8×9	4.3	6.3	71.4	13

2 缺陷特征提取与优化

超声波的声速、衰减、声阻抗、反射和散射等特性为超声波检测提供了丰富的信息. 物体中的缺陷如气孔、夹渣、裂纹、未熔合和未焊透等都将改变超声波的波形、幅值、相位、频谱、传播时间等,即超声检测回波携带了物体中缺陷体的大量信息. Case 等人[4]研究了缺陷的回波及频谱,并从中提取了相应的特征值. 采用人工智能方法进行缺陷的识别与判断,就必须首先了解各种缺陷的超声回波特征,并提取出能反映不同缺陷类别的特征.

2.1 超声回波信号特征提取

人们最熟悉的超声信号特征是表现在时域的超声回波波形特征. 由于不同缺陷反射体的大小、取向及表面状态等的不同,必然使得超声检测回波信号在时域上有所体现. 文中提取了缺陷回波信号的 14 个时域特征值,见表 2.

表 2 时域特征值

Table 2 Features in time domain

序列	特征值描述
1	回波包络线上升沿从 20% 峰值到 90% 峰值的上升时间
2	回波包络线下降沿从 90% 峰值到 20% 峰值的下降时间
3	回波包络线 20% 峰值之间的持续时间(振动时间)
4	回波包络线 50% 峰值之间的持续时间
5	回波包络线 90% 峰值之间的持续时间
6	回波包络线上升沿从 20% 峰值到 90% 峰值覆盖的上升面积
7	回波包络线下降沿从 90% 峰值到 20% 峰值覆盖的下降面积
8	上升面积与下降面积的比值
9	回波信号在振动时间内的平均能量(归一化能量)
10	回波信号的标准偏差
11	回波包络线的轮廓长度与轮廓线包围面积的比值(形状系数)
12	回波信号的陡峭度(峰度系数)
13	回波信号的对称性参数(当信号波形对称时为零)
14	回波包络线上各点的幅度均值

随着频谱分析技术的发展,通过研究信号在频域上的各种特性,提供了获得更多有用信息的机会. 通过对信号的频谱分析,提取了缺陷回波信号的 8 个频域特征值,见表 3.

表 3 频域特征值

Table 3 Features in frequency domain

序列	特征值描述
1	回波频谱的峰值频率
2	回波频谱的中心频率
3	回波频谱的带宽,即 -6dB 处的频谱宽度
4	回波频谱上升沿从 20% 峰值到 90% 峰值持续的低频分量
5	回波频谱下降沿从 90% 峰值到 20% 峰值持续的高频分量
6	回波频谱上升沿从 20% 峰值到 90% 峰值覆盖的低频面积
7	回波频谱下降沿从 90% 峰值到 20% 峰值覆盖的高频面积
8	高频面积与低频面积的比值

小波分析是一种时频分析方法,它突破了傅里叶变换在时域没有任何分辨力的限制,具有多分辨力分析的特点,广泛的应用于超声信号处理过程中. 小波包分析则是一种比小波分析更为精细的分解方

法，可将信号分解到不同的频带内. 由于不同缺陷能引起某些频带超声能量的不同，因此不同频带的能量会携带有不同缺陷类别的特征信息. 研究选用 sym10 小波基对缺陷信号进行了 4 层小波包分解，最终获得 16 个频带信号. 为了衡量缺陷的信号能量在各个频带上的分布情况，计算了第四层上各个节点的能量，从而获得各节点能量与第四层总能量的比值，得到一个 16 维的特征向量$\{A_1, A_2, A_3, \cdots, A_{16}\}$，并将其作为缺陷回波的时频域特征值，其中 A_k 可由式(1)计算获得，即

$$A_k = \frac{E_{4,j}}{E_4} = \frac{E_{4,j}}{\sum_{j=0}^{n} E_{4,j}}$$

$$j = 0,1,2,\cdots 15;\ k = 1,2,3,\cdots 16 \qquad (1)$$

式中：A_k 为第 k 个节点能量与第 4 层总能量比值，$E_{4,j}$ 为第 4 层上第 j 个频带的能量；E_4 为第 4 层上各节点的总能量.

2.2　超声图像形态特征提取

基于 USB 摄像头定位的超声成像检测系统不仅可以提供缺陷的三维成像，而且能够获得缺陷的尺寸、位置和形态等信息，这为缺陷的识别提供了一条不同于信号分析的道路. 焊缝中不同的缺陷，其位置、尺寸、姿态各有所不同. 比如体积型缺陷的投影成像尺寸一般较面型缺陷的成像尺寸要小. 在缺陷位置分布上，未焊透缺陷一般位于焊缝根部，而未熔合缺陷则一般位于焊缝侧壁. 因此从缺陷的三维投影图像入手，提取了缺陷图像的 7 个形态特征，见表 4，其定义如图 3 所示.

表 4　形态特征值

Table 4　Morphological features

序列	特征值描述
1	缺陷的自身长度 L
2	缺陷的自身宽度 H
3	缺陷的长宽比 $R = L/H$
4	缺陷到焊缝中心的距离 D
5	缺陷的取向 k
6	位于焊缝中心线左侧的缺陷比例 r_1
7	位于焊缝中心线右侧的缺陷比例 r_2

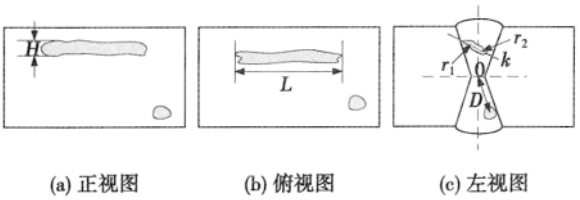

(a) 正视图　(b) 俯视图　(c) 左视图

图 3　形态特征提取示意图

Fig. 3　Schematic of morphological feature extraction

2.3　特征值评价与优化

特征优化的目的是降低特征向量空间的维数，减轻模式识别的计算容量，同时去除特征向量中的冗余信息，为模式识别提供更有效的特征量，提高模式识别的准确性和可靠性. 因此，对提取的特征向量进行合理的评价与优化是非常必要的. 大量研究[5-7]普遍认为，基于欧式距离的评价准则是一种非常直观的评价方法，能够有效的实现特征值的评价与优化. 为此利用基于欧式距离的评价准则，对文中提取的所有特征值分别进行了评价，图 4 给出了每个特征值的评价结果. 具体构建的评价公式为

$$J_d = tr(S_b)\ /tr(S_\omega) \qquad (2)$$

式中：J_d 为评价因子；tr 为矩阵的迹；S_b 为 c − 类样本的类间散度矩阵；S_ω 为 c − 类样本的类内散度矩阵.

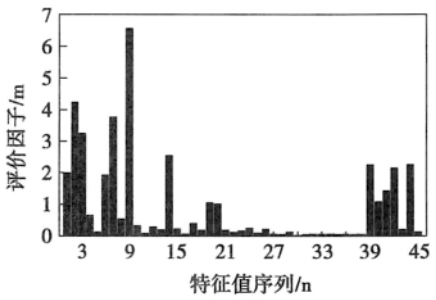

图 4　特征值评价示意图

Fig. 4　Schematic of feature evaluation

由评价公式可知，类内散度矩阵的迹越小，类间散度矩阵的迹越大，即 J_d 的数值越大，表明特征值对于缺陷的模式识别越有效. 据此选取了 14 个特征值($J_d > 1$)作为优化的特征子集，进一步计算了优选特征子集对于 5 类缺陷样本的基于欧式距离的类内、类间距，计算结果如表 5 所示.

表 5　五类缺陷的类内类间距离(mm)

Table 5　Distance in and between five kinds of flaws

缺陷类型	气孔	夹渣	裂纹	未焊透	未熔合
气孔	0.745	1.081	1.028	1.154	1.274
夹渣	1.081	0.724	1.333	1.503	1.608
裂纹	1.028	1.333	0.432	0.597	0.975
未焊透	1.154	1.503	0.597	0.562	0.925
未熔合	1.274	1.608	0.975	0.925	0.577

从表 5 中可以直观的看到，对角线上的距离数值最小，即同类缺陷的类内距离小于任何两个不同类缺陷的类间距离. 分析可见，优选的特征子集对于 5 类缺陷的分类识别是有效的.

3 缺陷的识别结果

近年来,神经网络技术在数据融合领域得到了广泛的应用,从数据融合的角度来看,神经网络可以看作一个融合系统,利用神经元之间不同的连接方式及算法可以构成不同的融合系统. BP 神经网络是一种基于误差反相传播的多层反馈网络,被广泛的用作信号的模式识别. 因此文中选用 BP 神经网络作为融合分类器,实现缺陷超声信号特征与图像形态特征的特征层数据融合,进行缺陷的智能识别,构建的融合分类器如图 5 所示.

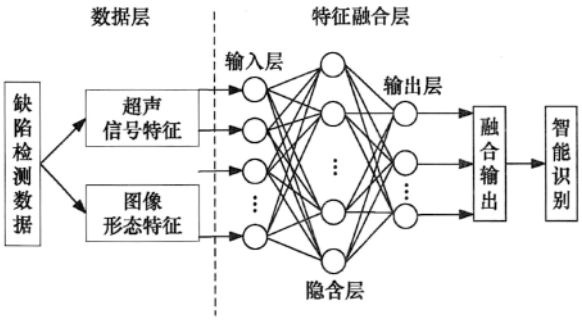

图 5 特征层融合分类器示意图

Fig. 5 Schematic of classifier of feature fusion

首先将 9 个优化的超声信号特征子集与 5 个优化的图像形态特征子集作为 BP 神经网络的输入端,对 128 个含有气孔、夹渣、裂纹、未焊透和未熔合 5 类典型焊接缺陷的样本进行了特征层融合的智能识别,识别结果见表 6.

表 6 基于特征融合的识别结果(%)

Table 6 Recognition results based on feature fusion

缺陷类型	气孔	夹渣	裂纹	未焊透	未熔合	综合
识别结果	100	90	100	90	90	94

为了与常规的基于超声信号特征的 BP 网络模式识别作对比,将 9 个优化的超声信号特征子集输入神经网络,对同样的 128 个缺陷样本进行了识别分类,识别结果见表 7. 对比结果表明,该方法有效的提高了缺陷的识别率,尤其是提高了裂纹和未焊透两类危害性最大的焊缝缺陷的检出率,有助于焊缝质量的评定.

表 7 基于信号特征的识别结果(%)

Table 7 Recognition results based on signal feature

缺陷类型	气孔	夹渣	裂纹	未焊透	未熔合	综合
识别结果	80	80	60	50	80	70

4 结 论

(1) 研究了一种基于超声信号和图像融合的焊缝缺陷识别新方法. 该方法充分利用检测数据,通过对缺陷回波信号特征与缺陷形态特征的数据融合,实现了焊缝缺陷的有效识别.

(2) 利用 BP 神经网络作为融合分类器,实现缺陷超声信号特征与图像形态特征的特征层数据融合,识别 5 类焊接缺陷. 与常规的基于超声信号特征的识别结果相比,该方法有效的提高了缺陷的识别率,有助于焊缝质量的评定.

参考文献:

[1] 王云平. 超声无损检测与评价的关键技术问题及解决方案[J]. 煤矿机械, 2008, 9: 194 - 196.
Wang Yunping. Key technical problems and solutions of ultrasonic nondestructive test and evaluation [J]. Coal Mine Machinery, 2008, 9: 194 - 196.

[2] 黄 民, 李 功. 焊缝超声无损检测中的缺陷智能识别方法[J]. 北京信息科技大学学报, 2009, 24(2): 33 - 36.
Huang Min, Li Gong. Intelligent defect recognition methods in the ultrasonic non-destructive test of welds [J]. Journal of Beijing Information Science and Technology University, 2009, 24(2): 33 - 36.

[3] 胡文刚, 刚 铁, 汪金海. 基于视频定位的焊缝缺陷超声检测技术[J]. 焊接学报, 2011, 32(9): 49 - 52.
Hu Wengang, Gang Tie, Wang Jinhai. Ultrasonic testing technology of weld defect based on video positioning [J]. Transactions of the China welding Institution, 2011, 32(9): 49 - 52.

[4] Case T J, Waag R C. Flaw identification from time and frequency features of ultrasonic waveforms [J]. IEEE Transactions on Ultrasonics Ferroelectrics and Frequency Control, 1996, 43(4): 592 - 600.

[5] Duda R O, Hart R E, Stork D G. Pattern classification [M]. Hoboken: Wiley, 2001.

[6] Brereton R G. Chemometrics: Data analysis for the laboratory and chemical plant [M]. Hoboken: Wiley, 2003.

[7] Lei Y G, He Z J, Zi Y Y. Application of an intelligent classification method to mechanical fault diagnosis [J]. Expert Systems with Applications, 2009, 36: 9941 - 9948.

作者简介: 胡文刚,男,1981 年出生,博士研究生. 主要从事焊接无损检测方面的研究. 发表论文 4 篇. Email: huwengang0105@163.com

通讯作者: 刚 铁,男,教授,博士研究生导师. Email: gangt@hit.edu.cn

of welding torch and the change of arc length was deduced, and a mathematical model was established for the arc length. Considering the characteristics and complexity of welding arc signal, the Gabor wavelet filter was used to eliminate the noise interference, and the feature vector was extracted from the sample data after filtering, and the dimension of data was reduced. The classifier of welding torch attitude according to the principle of Euclidean distance, real-time identification of the spatial attitude of welding torch was conducted with the steepest descent method of model parameters. The results show that the algorithm for recognition of spatial attitude of welding torch with swing of rotating arc sensor was simple and provided theoretical basis for improving the precision of welding seam tracking.

Key words: spatial attitude; welding torch; rotating arc; arc sensor; welding seam tracking

Low temperature sintering-bonding through in-situ formation of Ag nanoparticles using micro-scaled Ag_2O composite paste MU Fengwen[1], ZOU Guisheng[1], ZHAO Zhenyu[1], WU Aiping[1], YAN Jiuchun[2], Y. Norman Zhou[1,3] (1. Key Laboratory for Advanced Materials Processing Technology (Ministry of Education), Department of Mechanical Engineering, Tsinghua University, Beijing 100084, China; 2. State Key Laboratory of Advanced Welding & Joining, Harbin Institute of Technology, Harbin 150001, China; 3. Department of Mechanical and Mechatronics Engineering, University of Waterloo, Waterloo N2L 3G1, Canada). pp 38 - 42

Abstract: In order to reduce the cost of using Ag nanoparticle paste as bonding materials in electronic packaging, micro-scaled Ag_2O powders were mixed with triethylene glycol (TEG) to form a paste to replace the Ag particle paste. The reaction mechanism of in-situ formation of Ag nanoparticles, the sintering characteristics of micro-Ag_2O paste at low temperature, and the bonding of Ag-coated Cu bulks using this paste were investigated. The results reveal that the Ag_2O particles in the paste were more easily transformed into Ag nanoparticles than micro-Ag_2O itself, and with increasing the sintering temperature, more Ag nanoparticles formed and grew larger by sintering, accompanied with some gaseous products which could escape easily. The effect of sintering-bonding time on the strength of joints fabricated at 250 ℃ under a pressure of 2 MPa was analyzed. The average shear strength of the joints increased with sintering-bonding time and reached about 24 MPa when the sintering-bonding time was 5 min. And the microstructure of the fractured surface and the cross-section of typical joints made at 250 ℃ under 2 MPa were also examined.

Key words: silver oxide; in-situ formation; Ag nanoparticles; sintering bonding

Diagnosis of welding arc ionization region and boundary XIAO Tianjiao, SONG Yonglun, LI Chao, YAN Sibo (School of Mechanical Engineering and Applied Electronics Technology, Beijing University of Technology, Beijing 100123, China). pp 43 - 47

Abstract: Welding arc, as a heat source, converts electric energy to heat energy by gas discharging, and the scale of the arc ionization region as well as the effective range of the arc determines the distribution of its energy density. In this paper, the quantitative detection of argon atoms and argon-ion line intensity were achieved by emission spectroscopy diagnostic method, and the arc ionization region and the gas atom excitation radiation boundary scale were obtained. The measurement not only overcame the problem that the arc could not be quantitatively tested with camera due to exposure factors, but also could be used for observation of pulsed arc. The results provide the basis for better understanding arc physics and modeling the arc.

Key words: tungsten inert gas welding; arc boundary; ionization region; arc geometric pattern; spectroscopy diagnostic

Corrosion and wear behavior of wire-arc sprayed Ni-based coatings ZHAO Xiaozhou[1], ZHOU Zheng[1], HE Dingyong[1], ZHAO Qiuying[2], LI Ran[1], JIANG Jianmin[1] (1. College of Materials Science and Engineering, Beijing University of Technology, Beijing 100124, China; 2. Postdoctoral Research Station of Mechanical Engineering, Beijing University of Technology, Beijing 100124, China). pp 48 - 52

Abstract: A new Ni-based cored wire was designed to prepare coatings by wire-arc spraying on SA 213-T2 substrate in order to solve the corrosion and wear problems in waste-to-energy (WTE) plants. According to X-ray diffractometry (XRD) and scanning electron microscopy (SEM) analysis, the as-deposited coatings with low content of oxide phases presented uniform and dense layered structure with porosity at around 3%. The wear resistance of the designed coating, about 7 times higher than that of the substrate, was measured by a rubber wheel abrisive testing machine. Thermo-gravimetric technique was used to investigate the high-temperature corrosion behavior of the coatings in molten salt environment (Na_2SO_4 - 10% NaCl) at 800 ℃ in a muffle furnace. As a result, the weight gain curve of the coating followed the parabolic law and presented extremely lower corrosion rates, comparing with that of the substrate, due to the formation of Cr_2O_3 and $NiCr_2O_4$ oxide films on the surface which prevented the diffusion or penetrating of corrosive species. Consequently, the developed coating could provide much better corrosion resistance properties than SA213-T2 substrate.

Key words: Ni-based coating; arc spraying; microstructure; hot corrosion; wear behavior

Recognition of weld flaw based on feature fusion of ultrasonic signal and image HU Wengang, GANG Tie (State Key Laboratory of Advanced Welding and Joining, Harbin Institute of Technology, Harbin 150001, China). pp 53 - 56

Abstract: Ultrasonic testing is widely applied to detect the inner flaws of materials, but it is still difficult to recognize the flaw properties. In this paper, a new method for flaw recognition based on feature fusion of ultrasonic signal and image was proposed. The detection data was used to identify the weld flaw by the data fusion of ultrasonic signal feature and morphological feature. The welds containing defects such as hole, slag, crack,

lack of penetration and lack of fusion were inspected with the manual ultrasonic testing system. Then the ultrasonic signal features of flaw echo and morphological features of flaw image were extracted respectively. Finally, BP neural network was used to carry out the data fusion of these features. The results show that the multi-class flaws could be identified effectively, and the recognition rate of weld flaws was improved by this method.

Key words: ultrasonic testing; flaw recognition; data fusion; neural network

Numerical simulation of effect of laser power and assistant gas on laser cutting ability WEN Peng[1,3], WANG Wei[2], TAN Xianghu[1], SHAN Jiguo[1,3], WANG Xuyou[2], LIN Shangyang[2] (1. Department of Mechanical Engineering, Tsinghua University, Beijing 10084, China; 2. Harbin Welding Institute, China Academy of Machinery Science & Technology, Harbin 150080, China; 3. Key Laboratory of Advanced Materials, Ministry of Education, Beijing 100084, China). pp 57 - 60

Abstract: Materials were cut with the coupled interaction of laser power and assistant gas during laser cutting process. A multiphase flow model was established, which was able to reflect the interaction among laser energy, assistant gas and workpiece during laser cutting based on computational fluid dynamics. A hybrid heat source model was used, including laser power and oxygen-flow controlled combustion reaction heat. Low carbon steels were cut by fiber laser with O_2 or N_2 as assistant gas, and the cutting process was numerically simulated. The effect of laser power and assistant gas on laser cutting ability was investigated by regulating the laser power and gas pressure. The calculated results show that the laser cutting ability was determined by the coupled interaction of laser power and assistant gas. The numerical simulation can calculate both the temperature and flow fields, and can also predict the shape of cutting seam.

Key words: laser cutting; numerical simulation; temperature field; flow field; assistant gas

Weld formation characteristics in hybrid ultra-high frequency pulse variable polarity GTAW of 2219-T87 high strength aluminum alloy WANG Lexiao[1], CONG Baoqiang[1], LIU Fangjun[1], QI Bojin[1], YANG Mingxuan[1], LI Wei[1,2] (1. School of Mechanical Engineering and Automation, Beihang University, Beijing 100191, China; 2. Department of Electrical Engineering, Beijing Institute of Petro-Chemical Technology, Beijing 102617, China). pp 61 - 64

Abstract: The weld formation characteristics in the hybrid ultra-high frequency pulse variable polarity gas tungsten arc welding (HPVP-GTAW) of 2219-T87 high strength aluminum alloy was investigated. The experimental results show that, under the condition of keeping the RMS of positive current approximately consistent (with permissible variation of ±5 A), welding with ultra-high frequency pulse square-wave current increased the ratio of weld depth to width by more than 20%, compared with the traditional variable polarity GTAW process. Pulse current frequency significantly affected the weld formation. Increasing the pulse current amplitude and decreasing the pulse current duty cycle within a certain range can remarkably enhance the weld penetration. The ratio of weld depth to width increased by more than 75% when the pulse current was 100 A and the pulse current duty cycle was 20%.

Key words: high strength aluminum alloy; ultra-high frequency pulse current; variable polarity gas tungsten arc welding; weld formation

Fatigue life prediction of aluminum alloy welded joint based on variable precision rough set ZOU Li[1], YANG Xinhua[2], SUN Yibo[2], DENG Wu[1] (1. Software Institute, Dalian Jiaotong University, Dalian 116052, China; 2. School of Materials Science and Engineering, Dalian Jiaotong University, Dalian 116028, China). pp 65 - 68

Abstract: A model with variable precision rough set (VPRS) was established to predict the fatigue life of aluminum alloy welded joints. The main steps and the key issues were described, and the united entropy-based discretization algorithm and attribute reduction algorithm were used to process the data. The results show that the developed model had high accuracy and coverage with a certain noise tolerance. This method broadens the application of rough set theory and provides a new way to predict the fatigue life of welded joints.

Key words: variable precision rough set; welding structure; fatigue life

Motion simulation of open-arc welding robot based on ADAMS/View HAN Xing, LI Chang, YU Xiaoguang, ZHAO Guangbing (School of Mechanical Engineering & Automation, University of Science and Technology Liaoning, Anshan 114051, China). pp 69 - 72

Abstract: Open arc welding robot has been widely used in metallurgical industry, and the transmission accuracy of each component inevitably causes cumulative errors on running accuracy of the welding gun head and influences the welding quality. Therefore, how to improve the driven accuracy and control manufacture errors are key problems in welding robot design. In this paper, a virtual model of open-arc robot was built based on ADAMS/View, and after motion simulation, the robot dynamic characters were obtained in welding process. The results show that this new method was simple and highly accurate, without needing to establish complicated mathematic model, largely improves the design efficiency.

Key words: arc welding robot; simulation; ADAMS/View

Longitudinal calibration of welding pool altitude measuring system for gas tungsten arc welding HU Xian, LIU Nansheng, WEI Sheng, WEI Yiqing (Department of Physics, Nanchang University, Nanchang 330031, China). pp 73 - 76

Abstract: A longitudinal calibration method was proposed for welding pool altitude measuring system for tungsten inert gas welding, based on Fourier transform profilometry (FTP). A sinusoidal grating was projected to the calibration panel located in the welding pool, and the panel was longitudinally driven by a one-dimensional precise moving apparatus to construct diverse al-